doi:10.1038/nature23004

Global Λ hyperon polarization in nuclear collisions

The STAR Collaboration*

The extreme energy densities generated by ultra-relativistic collisions between heavy atomic nuclei produce a state of matter that behaves surprisingly like a fluid, with exceptionally high temperature and low viscosity[1]. Non-central collisions have angular momenta of the order of 1,000$\hbar$, and the resulting fluid may have a strong vortical structure[2–4] that must be understood to describe the fluid properly. The vortical structure is also of particular interest because the restoration of fundamental symmetries of quantum chromodynamics is expected to produce novel physical effects in the presence of strong vorticity[5]. However, no experimental indications of fluid vorticity in heavy ion collisions have yet been found. Since vorticity represents a local rotational structure of the fluid, spin–orbit coupling can lead to preferential orientation of particle spins along the direction of rotation. Here we present measurements of an alignment between the global angular momentum of a non-central collision and the spin of emitted particles (in this case the collision occurs between gold nuclei and produces Λ baryons), revealing that the fluid produced in heavy ion collisions is the most vortical system so far observed. (At high energies, this fluid is a quark–gluon plasma.) We find that Λ and $\overline{\Lambda}$ hyperons show a positive polarization of the order of a few per cent, consistent with some hydrodynamic predictions[6]. (A hyperon is a particle composed of three quarks, at least one of which is a strange quark; the remainder are up and down quarks, found in protons and neutrons.) A previous measurement[7] that reported a null result, that is, zero polarization, at higher collision energies is seen to be consistent with the trend of our observations, though with larger statistical uncertainties. These data provide experimental access to the vortical structure of the nearly ideal liquid[8] created in a heavy ion collision and should prove valuable in the development of hydrodynamic models that quantitatively connect observations to the theory of the strong force.

The primary objective of the Relativistic Heavy Ion Collider (RHIC) at Brookhaven National Laboratory is to produce a large (relative to the size of a proton) system of matter at temperatures of $T \approx 200\,\mathrm{MeV}/k_\mathrm{B} \approx 2.3 \times 10^{12}\,\mathrm{K}$ by colliding gold nuclei travelling at 96.3% to 99.995% of the speed of light. Such temperatures, more than 100,000 times that at the Sun's core, characterized the Universe only a few microseconds after the Big Bang[9]. Under these extreme conditions, the protons and neutrons that comprise our everyday world melt into a state of deconfined quarks and gluons called the quark–gluon plasma[1,10]. Before RHIC was turned on in 1999, the expectation was that this plasma would be weakly coupled and highly viscous. However, the discovery of strong collective behaviour led to the surprising conclusion that the system generated in these collisions was in fact a liquid with the lowest ratio of viscosity to entropy density ever observed[8].

Since then, a large programme of experimental investigation combined with increasingly sophisticated hydrodynamic theory have succeeded in reproducing observed properties of the fluid[11]. A complete understanding of this fluid may provide deep insights into the strongest and most poorly understood of the fundamental forces in nature. Quantum chromodynamics is the theory of the strong interactions between quarks and gluons, but experimental input from RHIC is essential to understand quark confinement and the origin of hadron mass.

A collaboration of physicists from 13 countries operates the STAR detector system[12], which has recorded billions of collisions at RHIC. A rendering of the STAR experiment is shown in Fig. 1. Opposing beams of gold nuclei collide in the centre of the time projection chamber (TPC), generating a spray of charged particles. The TPC signal from a single event is shown in Fig. 2. Forward- and backward-travelling particles and fragments that experience only a small deflection are measured in the beam–beam counters.

Most collisions at RHIC are not head-on, and so involve substantial angular momentum, of the order of 1,000 $\hbar$ (where $\hbar$ is the reduced Planck constant) for a typical collision. A slight sideward deflection of the forward- and backward-travelling fragments[13] from a given collision allows experimental determination of the direction of the overall angular momentum $\hat{J}_{\mathrm{sys}}$. as shown schematically in Fig. 3.

Recently, Takahashi *et al.*[14] reported the first observation of a coupling between the vorticity of a fluid and the internal quantum spin of the electron, opening the door to a new field of fluid spintronics. In their study, the vorticity $\boldsymbol{\omega}$—a measure of the 'swirl' of the velocity flow field around any point (non-relativistically, $\boldsymbol{\omega} = \frac{1}{2}\nabla \times \boldsymbol{v}$)—is generated through shear viscous effects as liquid mercury flows next to a rigid wall.

In a heavy ion collision, shear forces generated by the interpenetrating nuclei may present an analogous situation, introducing vorticity to the fluid. Indeed, hydrodynamic calculations[15] with initial conditions tuned to reproduce measured momentum anisotropies predict tremendous vorticity in the fluid at RHIC. So far, no experimental evidence of vorticity at RHIC has been reported, and its role in the evolution of the fluid has not been explored extensively at the theoretical level.

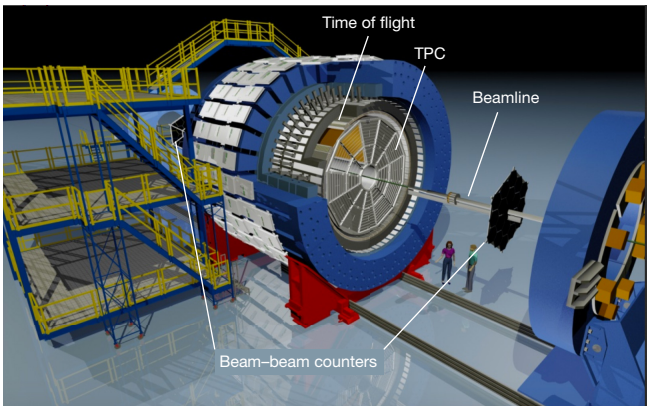

Figure 1 | The STAR detector system. Gold nuclei travelling at nearly the speed of light travel along the beamline and collide in the centre of the detector system. Charged particles emitted at mid-rapidity (that is, having a relatively small component of velocity along the beam direction) are measured in the TPC (see also Fig. 2) and the time-of-flight detectors. Forward- and backward-going beam fragments are detected in the beam–beam counters.

*A list of participants and their affiliations appears at the end of the paper.

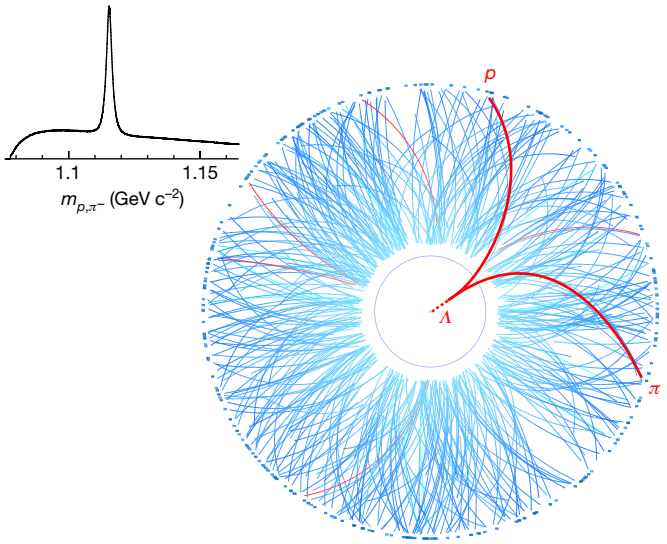

Figure 2 | A single Au + Au collision in the STAR TPC. Charged particles from a collision ionize the gas in the TPC, forming tracks that curve in the magnetic field of the detector. The tracks are reconstructed in three dimensions, making them relatively easy to distinguish, but are projected onto a single plane in this figure. As the tracks exit the outer radius, they leave a signal in the time-of-flight detector. The species of charged particles is determined by the amount of ionization in the TPC and the flight time as measured by time of flight. Charged daughters from the weak decay $\Lambda \to p + \pi^-$ are extrapolated backwards, and the parent is identified through topological selection. A clear peak at the Λ mass, obtained by summing over many events, is observed in the invariant-mass distribution m_{p,π^-}.

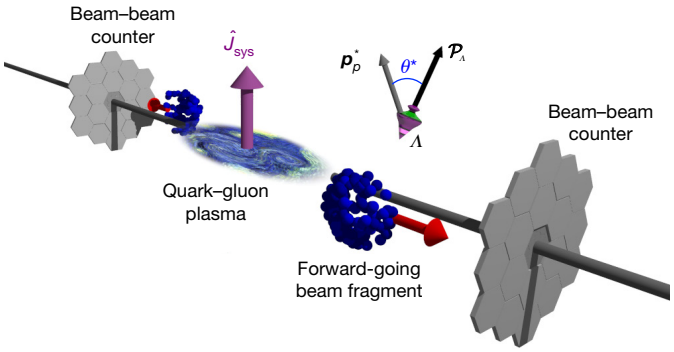

Figure 3 | A sketch of a Au + Au collision in the STAR detector system. The vorticity of fluid created at mid-rapidity is suggested. The average vorticity points along the direction of the angular momentum of the collision $\hat{J}_{sys}$. This direction is estimated experimentally by measuring the sidewards deflection of the forward- and backward-going fragments and particles in the beam–beam counter detectors. Λ hyperons are depicted as spinning tops; see text for details. Obviously, elements in this depiction are not drawn to scale: the fluid and beam fragments have sizes of a few femtometers, whereas the radius of each beam–beam counter is about 1 m.

The vorticity is currently of intense interest, since it is a key ingredient in theories that predict observable effects associated with chiral symmetry restoration and the production of false quantum chromodynamics vacuum states[5]. Spin–orbit coupling can generate a spin alignment, or polarization, along the direction of the vorticity in the local fluid cell, which, when averaged[2,3] over the entire system, is parallel to $\hat{J}_{sys}$. Thus, polarization measurements of hadrons emitted from the fluid can be used to determine $\omega \equiv |\boldsymbol{\omega}|$.

It is difficult to measure the spin direction of most hadrons emitted in a heavy ion collision. However, Λ and $\overline{\Lambda}$ hyperons are 'self-analysing'. That is[16], in the weak decay $\Lambda \to p + \pi^-$, the proton tends to be emitted along the spin direction of the parent Λ. If θ^* is the angle between the daughter proton (antiproton) momentum $\boldsymbol{p}_p^*$ and the Λ ($\overline{\Lambda}$) polarization vector $\boldsymbol{\mathcal{P}}_H$ in the hyperon rest frame, then

$$\frac{dN}{d\cos\theta^*} = \frac{1}{2}(1 + \alpha_H |\boldsymbol{\mathcal{P}}_H| \cos\theta^*) \quad (1)$$

The subscript H denotes Λ or $\overline{\Lambda}$, and the decay parameter[17] $\alpha_\Lambda = -\alpha_{\overline{\Lambda}} = 0.642 \pm 0.013$. The angle θ^* is indicated in Fig. 3, in which Λ hyperons are depicted as tops spinning about their polarization direction.

The polarization of the hyperon in its rest frame depends on the vorticity of the fluid element (in the laboratory frame[3,18]) and thus may depend on the momentum of the emitted hyperons. However, when averaged over all phase space, symmetry demands that $\boldsymbol{\mathcal{P}}_H$ is parallel to $\hat{J}_{sys}$. Because our limited sample sizes prohibit exploration of these dependencies, our analysis assumes that $\boldsymbol{\mathcal{P}}_H$ is independent of momentum, and we extract only an average projection of the polarization on $\hat{J}_{sys}$. This average may be written[7] as

$$\overline{\mathcal{P}}_H \equiv \langle \boldsymbol{\mathcal{P}}_H \cdot \hat{J}_{sys} \rangle = \frac{8}{\pi \alpha_H} \frac{\left\langle \cos\left(\phi_p^* - \phi_{\hat{J}_{sys}}\right) \right\rangle}{R_{EP}^{(1)}} \quad (2)$$

where $\phi_{\hat{J}_{sys}}$ is the azimuthal angle of the angular momentum of the collision, ϕ_p^* is the azimuthal angle of the daughter proton (antiproton) momentum in the Λ ($\overline{\Lambda}$) rest frame, and $R_{EP}^{(1)}$ is a factor that accounts for the finite resolution[7] with which we determine $\phi_{\hat{J}_{sys}}$. The overbar on $\mathcal{P}_H$ denotes an average over events and the angle brackets denote the momenta of Λ hyperons detected in the TPC. Equation (2) is strictly valid only in a perfect detector; angle-dependent detection efficiency requires a correction factor[7] that shifts the results in the present analysis by about 3%.

A relativistic heavy ion collision can produce several hundred charged particles in our detectors. For a given energy, a head-on collision produces the maximum number of emitted particles, while a glancing one produces only a few. To concentrate on collisions with sufficient overlap to produce a fluid with large angular momentum, we select events producing an intermediate number of tracks in the TPC. Of all observed collisions 20% produce more tracks than the collisions studied here, while 50% produce fewer; in the parlance of the field, this is known as a 20–50% centrality selection.

Equation (2) quantifies an average alignment between hyperon spin and a global feature of the collision and is hence a "global polarization"[2]. This is distinct from the well known phenomenon of Λ polarization at very forward angles in proton–proton collisions[19]. The polarization direction from this latter effect depends on Λ momentum and not the global angular momentum; it has zero magnitude at mid-rapidity.

The solid symbols in Fig. 4 show our new measurements as a function of collision energy, $\sqrt{s_{NN}}$. Systematic uncertainties are shown as boxes and are generally smaller than statistical ones. Λ hyperons in the rapidity region $|y_\Lambda| < 1.0$ and transverse momentum $0.4 < p_T < 3.0$ GeV/c are used in the analysis. The peak in the invariant mass distribution at m_Λ is about five times the background level, and the integrated Λ contribution in our selected mass window is about twice that of the combinatoric background. Our results have been corrected for the 'diluting' effect of this combinatoric background. At each energy, a positive polarization at the level of 1.1–3.6 times the statistical uncertainty is observed for both Λ and $\overline{\Lambda}$. Taken in aggregate, the data are statistically consistent with the hypothesis of energy-independent polarization of 1.08 ± 0.15 (stat) ± 0.11 (sys) and 1.38 ± 0.30 (stat) ± 0.13 (sys) per cent for Λ and $\overline{\Lambda}$, respectively. Some models predict that the polarization may decrease with collision energy[4,20,21]. While our data are consistent with such a trend, increased statistics would be required to test these predictions definitively. Also shown as open symbols in Fig. 4 are previously published[7] measurements at $\sqrt{s_{NN}} = 62.4$ GeV and 200 GeV. The null result reported[7] may be seen

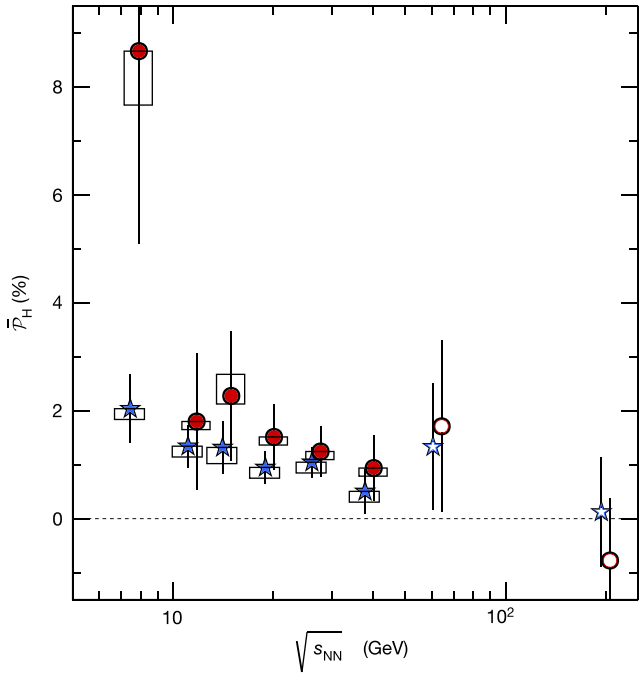

Figure 4 | The hyperon average polarization in Au + Au collisions. The average polarization for Λ (blue stars) and $\overline{\Lambda}$ (red circles) from 20–50% central collisions are plotted as a function of collision energy. Error bars represent statistical uncertainties only, while boxes represent systematic uncertainties. The results of the present study ($\sqrt{s_{NN}} < $ GeV), indicated by filled symbols, are shown together with those reported earlier[7] for 62.4 GeV and 200 GeV collisions, indicated by open symbols and for which only statistical errors are plotted.

as consistent with our measurements, within reported statistical uncertainty.

We have performed several checks that indicate a zero polarization 'signal', as expected, in the combinatoric background of proton–pion pairs that do not come from Λ hyperons. This includes analysis of proton–pion pairs with invariant masses slightly different from the mass of a Λ hyperon m_Λ. Nevertheless, these checks have finite statistical precision, so we consider the possibility of fluctuations in the background that could contribute to the polarization signal. This dominates the systematic uncertainties in the signal. Uncertainties due to Λ identification criteria (such as requirements for the spatial proximity of the proton and π daughters) are negligible. There are also small systematic uncertainties in the overall scale, which would scale both the value of $\overline{\mathcal{P}}_H$ and the statistical uncertainty, thus not affecting the statistical significance of the signal. These include the uncertainties in the Λ decay parameter α (2%)[17], the reaction-plane resolution (about 2%)[22], and detector efficiency corrections (about 3.5%).

The fluid vorticity may be estimated from the data using the hydrodynamic relation[18]

$$\omega \approx k_B T(\overline{\mathcal{P}}_{\Lambda'} + \overline{\mathcal{P}}_{\overline{\Lambda}'})/\hbar \quad (3)$$

where T is the temperature of the fluid at the moment when particles are emitted from it. The subscripts Λ' and $\overline{\Lambda}'$ in equation (3) indicate that these polarizations are for 'primary' hyperons emitted directly from the fluid. However, most of the Λ and $\overline{\Lambda}$ hyperons at these collision energies are not primary, but are decay products from heavier particles (for example, $\Sigma^{*,+} \to \Lambda + \pi^+$), which themselves would be polarized by the fluid. The data in Fig. 4 contain both primary and these 'feed-down' contributions. At these collision energies, the effect of feed-down is estimated[18] to produce differences of only about 20% between the polarization of primary and of all hyperons.

The $\sqrt{s_{NN}}$-averaged polarizations indicate a vorticity of $\omega \approx (9 \pm 1) \times 10^{21}\,s^{-1}$, with a systematic uncertainty of a factor of two, mostly owing to uncertainties in the temperature. This far surpasses the vorticity of all other known fluids, including solar subsurface flow[23] ($10^{-7}\,s^{-1}$); large-scale terrestrial atmospheric patterns[24] (10^{-7}–$10^{-5}\,s^{-1}$); supercell tornado cores[25] ($10^{-1}\,s^{-1}$); the great red spot of Jupiter[26] (up to $10^{-4}\,s^{-1}$); and the rotating, heated soap bubbles ($100\,s^{-1}$) used to model climate change[27]. Vorticities of up to $150\,s^{-1}$ have been measured in turbulent flow[28] in bulk superfluid He II, and Gomez *et al.*[29] have recently produced superfluid nanodroplets with $\omega \approx 10^7\,s^{-1}$.

Relativistic heavy ion collisions are expected to produce intense magnetic fields[30] parallel to $\hat{J}_{sys}$. Coupling between the field and the intrinsic magnetic moments of emitted particles may induce a larger polarization for $\overline{\Lambda}$ hyperons than for Λ hyperons[18]. This is not inconsistent with our observations, but probing the field will require more data to reduce statistical uncertainties as well as potential effects related to differences in the measured momenta of Λ and $\overline{\Lambda}$ hyperons.

The discovery of global Λ polarization in non-central heavy ion collisions opens up new directions in the study of the hottest, least viscous—and now, most vortical—fluid produced in the laboratory. Quantitative estimates of extreme vorticity yield a more complete characterization of the system and are crucial input to studies of phenomena related to chiral symmetry restoration that may provide insight into the complex interactions between quarks and gluons.

Online Content Any Extended Data display items and Source Data are available in the online version of the paper; references unique to these sections appear only in the online paper.

Data Availability The polarization data published here are available in the HEPdata repository http://dx.doi.org/10.17182/hepdata.77494.

Accepted 26 May 2017.

1. Adams, J. *et al.* Experimental and theoretical challenges in the search for the quark gluon plasma: the STAR Collaboration's critical assessment of the evidence from RHIC collisions. *Nucl. Phys. A* **757,** 102–183 (2005).
2. Liang, Z.-T. & Wang, X.-N. Globally polarized quark-gluon plasma in non-central A+A collisions. *Phys. Rev. Lett.* **94,** 102301 (2005); erratum **96**, 039901 (2006).
3. Becattini, F., Piccinini, F. & Rizzo, J. Angular momentum conservation in heavy ion collisions at very high energy. *Phys. Rev. C* **77,** 024906 (2008).
4. Pang, L.-G., Petersen, H., Wang, Q. & Wang, X.-N. Vortical fluid and Λ spin correlations in high-energy heavy-ion collisions. *Phys. Rev. Lett.* **117,** 192301 (2016).
5. Kharzeev, D. E., Liao, J., Voloshin, S. A. & Wang, G. Chiral magnetic and vortical effects in high-energy nuclear collisions: A status report. *Prog. Part. Nucl. Phys.* **88,** 1–28 (2016).
6. Becattini, F., Csernai, L. & Wang, D. J. Λ polarization in peripheral heavy ion collisions. *Phys. Rev. C* **88,** 034905 (2013).
7. Abelev, B. I. *et al.* Global polarization measurement in Au+Au collisions. *Phys. Rev. C* **76,** 024915 (2007); erratum **95,** 039906 (2017).
8. Heinz, U. & Snellings, R. Collective flow and viscosity in relativistic heavy-ion collisions. *Ann. Rev. Nucl. Part. Sci.* **63,** 123–151 (2013).
9. Kolb, E. W. & Turner, M. S. The early Universe. *Front. Phys.* **69,** 1–547 (1990).
10. Shuryak, E. V. Quantum chromodynamics and the theory of superdense matter. *Phys. Rep.* **61,** 71–158 (1980).
11. Csernai, L. P. & Stöcker, H. Global collective flow in heavy ion reactions from the beginnings to the future. *J. Phys. G* **41,** 124001 (2014).
12. Ackermann, K. H. *et al.* STAR detector overview. *Nucl. Instrum. Meth. A* **499,** 624–632 (2003).
13. Voloshin, S. A. & Niida, T. Ultrarelativistic nuclear collisions: direction of spectator flow. *Phys. Rev. C* **94,** 021901 (2016).
14. Takahashi, R. *et al.* Spin hydrodynamic generation. *Nat. Phys.* **12,** 52–56 (2016).
15. Becattini, F. *et al.* A study of vorticity formation in high energy nuclear collisions. *Eur. Phys. J. C* **75,** 406 (2015).
16. Pondrom, L. Hyperon experiments at Fermilab. *Phys. Rep.* **122,** 57–172 (1985).
17. Olive, K. A. *et al.* Review of particle physics. *Chin. Phys. C* **38,** 090001 (2014).
18. Becattini, F., Karpenko, I., Lisa, M., Upsal, I. & Voloshin, S. Global hyperon polarization at local thermodynamic equilibrium with vorticity, magnetic field, and feed-down. *Phys. Rev. C* **95,** 054902 (2017).
19. Bunce, G. *et al.* Λ^0 hyperon polarization in inclusive production by 300-GeV protons on beryllium. *Phys. Rev. Lett.* **36,** 1113–1116 (1976).
20. Betz, B., Gyulassy, M. & Torrieri, G. Polarization probes of vorticity in heavy ion collisions. *Phys. Rev. C* **76,** 044901 (2007).
21. Jiang, Y., Lin, Z.-W. & Liao, J. Rotating quark-gluon plasma in relativistic heavy ion collisions. *Phys. Rev. C* **94,** 044910 (2016).

22. Adamczyk, L. *et al.* Beam-energy dependence of the directed flow of protons, antiprotons, and pions in Au+Au Collisions. *Phys. Rev. Lett.* **112,** 162301 (2014).
23. Komm, R. *et al.* Divergence and vorticity of solar subsurface flows derived from ring-diagram analysis of MDI and GONG data. *Astrophys. J.* **667,** 571–584 (2007).
24. Perry, C. A. Midwestern streamflow, precipitation, and atmospheric vorticity influenced by Pacific sea-surface temperatures and total solar-irradiance variations. Int. *J. Clim.* **26,** 207–218 (2006).
25. Wurman, J. *et al.* Dual-Doppler analysis of winds and vorticity budget terms near a tornado. Mon. *Weath. Rev.* **135,** 2392–2405 (2007).
26. Choi, D., Banfield, D., Gierasch, P. & Showman, A. Velocity and vorticity measurements of Jupiter's Great Red Spot using automated cloud feature tracking. *Icarus* **188,** 35–46 (2007).
27. Meuel, T. *et al.* Intensity of vorticies: from soap bubbles to hurricanes. *Sci. Rep.* **3,** 1–7 (2013).
28. Donnelly, R. Quantized vorticies and turbulence in helium II. *Annu. Rev. Fluid Mech.* **25,** 325–371 (1993).
29. Gomez, L. F. *et al.* Shapes and vorticities of superfluid helium nanodroplets. *Science* **345,** 906–909 (2014).
30. Skokov, V., Illarionov, A. Yu. & Toneev, V. Estimate of the magnetic field strength in heavy-ion collisions. *Int. J. Mod. Phys. A* **24,** 5925–5932 (2009).

Acknowledgements We thank the RHIC Operations Group and RCF at Brookhaven National Laboratory, the NERSC Center at Lawrence Berkeley National Laboratory, and the Open Science Grid consortium for providing resources and support. This work was supported in part by the Office of Nuclear Physics within the US Department of Energy Office of Science, the US National Science Foundation, the Ministry of Education and Science of the Russian Federation, the National Natural Science Foundation of China, the Chinese Academy of Science, the Ministry of Science and Technology of China and the Chinese Ministry of Education, the National Research Foundation of Korea, the GA and MSMT of the Czech Republic, Department of Atomic Energy and Department of Science and Technology of the Government of India, the National Science Centre of Poland, the National Research Foundation, the Ministry of Science, Education and Sports of Croatia, and RosAtom of Russia.

Author Contributions All authors contributed extensively.

The STAR Collaboration

L. Adamczyk[1], J. K. Adkins[2], G. Agakishiev[3], M. M. Aggarwal[4], Z. Ahammed[5], N. N. Ajitanand[6], I. Alekseev[7,8], D. M. Anderson[9], R. Aoyama[10], A. Aparin[3], D. Arkhipkin[11], E. C. Aschenauer[11], M. U. Ashraf[12], A. Attri[4], G. S. Averichev[3], X. Bai[13], V. Bairathi[14], A. Behera[6], R. Bellwied[15], A. Bhasin[16], A. K. Bhati[4], P. Bhattarai[17], J. Bielcik[18], J. Bielcikova[19], L. C. Bland[11], I. G. Bordyuzhin[7], J. Bouchet[20], J. D. Brandenburg[21], A. V. Brandin[8], D. Brown[22], I. Bunzarov[3], J. Butterworth[21], H. Caines[23], M. Calderón de la Barca Sánchez[24], J. M. Campbell[25], D. Cebra[24], I. Chakaberia[11], P. Chaloupka[18], Z. Chang[9], N. Chankova-Bunzarova[3], A. Chatterjee[5], S. Chattopadhyay[5], X. Chen[26], J. H. Chen[27], X. Chen[28], J. Cheng[12], M. Cherney[29], W. Christie[11], G. Contin[30], H. J. Crawford[31], S. Das[13], L. C. De Silva[29], R. R. Debbe[11], T. G. Dedovich[3], J. Deng[32], A. A. Derevschikov[33], L. Didenko[11], C. Dilks[34], X. Dong[30], J. L. Drachenberg[35], J. E. Draper[24], L. E. Dunkelberger[36], J. C. Dunlop[11], L. G. Efimov[3], N. Elsey[37], J. Engelage[31], G. Eppley[21], R. Esha[36], S. Esumi[10], O. Evdokimov[38], J. Ewigleben[22], O. Eyser[11], R. Fatemi[2], S. Fazio[11], P. Federic[19], P. Federicova[18], J. Fedorisin[3], Z. Feng[13], P. Filip[3], E. Finch[39], Y. Fisyak[11], C. E. Flores[24], L. Fulek[1], C. A. Gagliardi[9], D. Garand[40], F. Geurts[21], A. Gibson[41], M. Girard[42], D. Grosnick[41], D. S. Gunarathne[43], Y. Guo[20], A. Gupta[16], S. Gupta[16], W. Guryn[11], A. I. Hamad[20], A. Hamed[9], A. Harlenderova[18], J. W. Harris[23], L. He[40], S. Heppelmann[34], S. Heppelmann[24], A. Hirsch[40], G. W. Hoffmann[17], S. Horvat[23], T. Huang[44], B. Huang[38], X. Huang[12], H. Z. Huang[36], T. J. Humanic[25], P. Huo[6], G. Igo[36], W. W. Jacobs[45], A. Jentsch[17], J. Jia[6,11], K. Jiang[26], S. Jowzaee[37], E. G. Judd[31], S. Kabana[20], D. Kalinkin[45], K. Kang[12], K. Kauder[37], H. W. Ke[11], D. Keane[20], A. Kechechyan, Z. Khan[38], D. P. Kikoła[42], I. Kisel[46], A. Kisiel[42], L. Kochenda[8], M. Kocmanek[19], T. Kollegger[46], L. K. Kosarzewski[42], A. F. Kraishan[43], P. Kravtsov[8], K. Krueger[47], N. Kulathunga[15], L. Kumar[4], J. Kvapil[18], J. H. Kwasizur[45], R. Lacey[6], J. M. Landgraf[11], K. D. Landry[36], J. Lauret[11], A. Lebedev[11], R. Lednicky[3], J. H. Lee[11], X. Li[26], C. Li[26], W. Li[27], Y. Li[12], J. Lidrych[18], T. Lin[45], M. A. Lisa[25], H. Liu[45], P. Liu[6], Y. Liu[9], F. Liu[13], T. Ljubicic[11], W. J. Llope[37], M. Lomnitz[30], R. S. Longacre[11], S. Luo[38], X. Luo[13], G. L. Ma[27], L. Ma[27], Y. G. Ma[27], R. Ma[11], N. Magdy[6], R. Majka[23], D. Mallick[14], S. Margetis[20], C. Markert[17], H. S. Matis[30], K. Meehan[24], J. C. Mei[32], Z. W. Miller[38], N. G. Minaev[33], S. Mioduszewski[9], D. Mishra[14], S. Mizuno[30], B. Mohanty[14], M. M. Mondal[48], D. A. Morozov[33], M. K. Mustafa[30], Md. Nasim[36], T. K. Nayak[5], J. M. Nelson[31], M. Nie[27], G. Nigmatkulov[8], T. Niida[37], L. V. Nogach[33], T. Nonaka[10], S. B. Nurushev[33], G. Odyniec[30], A. Ogawa[11], K. Oh[49], V. A. Okorokov[8], D. Olvitt Jr[43], B. S. Page[11], R. Pak[11], Y. Pandit[38], Y. Panebratsev[3], B. Pawlik[50], H. Pei[13], C. Perkins[31], P. Pile[11], J. Pluta[42], K. Poniatowska[42], J. Porter[30], M. Posik[43], A. M. Poskanzer[30], N. K. Pruthi[4], M. Przybycien[1], J. Putschke[37], H. Qiu[40], A. Quintero[43], S. Ramachandran[2], R. L. Ray[17], R. Reed[22], M. J. Rehbein[29], H. G. Ritter[30], J. B. Roberts[21], O. V. Rogachevskiy[3], J. L. Romero[24], J. D. Roth[29], L. Ruan[11], J. Rusnak[19], O. Rusnakova[18], N. R. Sahoo[9], P. K. Sahu, S. Salur[30], J. Sandweiss[23], M. Saur[19], J. Schambach[17], A. M. Schmah[30], W. B. Schmidke[11], N. Schmitz[51], B. R. Schweid[6], J. Seger[29], M. Sergeeva[36], P. Seyboth[51], N. Shah[27], E. Shahaliev[3], P. V. Shanmuganathan[22], M. Shao[26], A. Sharma[16], M. K. Sharma[16], W. Q. Shen[27], Z. Shi[30], S. S. Shi[13], Q. Y. Shou[27], E. P. Sichtermann[30], R. Sikora[1], M. Simko[19], S. Singha[20], M. J. Skoby[45], N. Smirnov[23], D. Smirnov[11], W. Solyst[45], L. Song[15], P. Sorensen[11], H. M. Spinka[47], B. Srivastava[40], T. D. S. Stanislaus[41], M. Strikhanov[8], B. Stringfellow[40], T. Sugiura[10], M. Sumbera[19], B. Summa[34], Y. Sun[26], X. M. Sun[13], X. Sun[13], B. Surrow[43], D. N. Svirida[7], A. H. Tang[11], Z. Tang[26], A. Taranenko[8], T. Tarnowsky[52], A. Tawfik[53], J. Thäder[30], J. H. Thomas[30], A. R. Timmins[15], D. Tlusty[21], T. Todoroki[11], M. Tokarev[3], S. Trentalange[36], R. E. Tribble[9], P. Tribedy[11], S. K. Tripathy, B. A. Trzeciak[18], O. D. Tsai[36], T. Ullrich[11], D. G. Underwood[47], I. Upsal[25], G. Van Buren[11], G. van Nieuwenhuizen[11], A. N. Vasiliev[33], F. Videbæk[11], S. Vokal[3], S. A. Voloshin[37], A. Vossen[45], G. Wang[36], Y. Wang[13], F. Wang[40], Y. Wang[12], J. C. Webb[11], G. Webb[11], L. Wen[36], G. D. Westfall[52], H. Wieman[30], S. W. Wissink[45], R. Witt[54], Y. Wu[20], Z. G. Xiao[12], W. Xie[40], G. Xie[26], J. Xu[13], N. Xu[30], Q. H. Xu[32], Y. F. Xu[27], Z. Xu[11], Y. Yang[44], Q. Yang[26], C. Yang[32], S. Yang[11], Z. Ye[38], Z. Ye[38], L. Yi[23], K. Yip[11], I. -K. Yoo[49], N. Yu[13], H. Zbroszczyk[42], W. Zha[26], Z. Zhang[27], X. P. Zhang[12], J. B. Zhang[13], S. Zhang[26], J. Zhang[28], Y. Zhang[26], J. Zhang[30], S. Zhang[27], J. Zhao[40], C. Zhong[27], L. Zhou[26], C. Zhou[27], X. Zhu[12], Z. Zhu[32] & M. Zyzak[46]

[1]AGH University of Science and Technology, FPACS, Cracow 30-059, Poland. [2]University of Kentucky, Lexington, Kentucky 40506-0055, USA. [3]Joint Institute for Nuclear Research, Dubna 141 980, Russia. [4]Panjab University, Chandigarh 160014, India. [5]Variable Energy Cyclotron Centre, Kolkata 700064, India. [6]State University of New York, Stony Brook, New York 11794, USA. [7]Alikhanov Institute for Theoretical and Experimental Physics, Moscow 117218, Russia. [8]National Research Nuclear University, MEPhI, Moscow 115409, Russia. [9]Texas A&M University, College Station, Texas 77843, USA. [10]University of Tsukuba, Tsukuba, Ibaraki, Japan. [11]Brookhaven National Laboratory, Upton, New York 11973, USA. [12]Tsinghua University, Beijing 100084, China. [13]Central China Normal University, Wuhan, Hubei 430079, USA. [14]National Institute of Science Education and Research, Bhubaneswar 751005, India. [15]University of Houston, Houston, Texas 77204, USA. [16]University of Jammu, Jammu 180001, India. [17]University of Texas, Austin, Texas 78712, USA. [18]Czech Technical University in Prague, FNSPE, Prague 115 19, Czech Republic. [19]Nuclear Physics Institute AS CR, Prague 250 68, Czech Republic. [20]Kent State University, Kent, Ohio 44242, USA. [21]Rice University, Houston, Texas 77251, USA. [22]Lehigh University, Bethlehem, Pennsylvania 18015, USA. [23]Yale University, New Haven, Connecticut 06520, USA. [24]University of California, Davis, California 95616, USA. [25]Ohio State University, Columbus, Ohio 43210, USA. [26]University of Science and Technology of China, Hefei, Anhui 230026, China. [27]Shanghai Institute of Applied Physics, Chinese Academy of Sciences, Shanghai 201800, China. [28]Institute of Modern Physics, Chinese Academy of Sciences, Lanzhou, Gansu 730000, USA. [29]Creighton University, Omaha, Nebraska 68178, USA. [30]Lawrence Berkeley National Laboratory, Berkeley, California 94720, USA. [31]University of California, Berkeley, California 94720, USA. [32]Shandong University, Jinan, Shandong 250100, China. [33]Institute of High Energy Physics, Protvino 142281, Russia. [34]Pennsylvania State University, University Park, Pennsylvania 16802, USA. [35]Physics Department, Lamar University, Beaumont, Texas 77710, USA. [36]University of California, Los Angeles, California 90095, USA. [37]Wayne State University, Detroit, Michigan 48201, USA. [38]University of Illinois at Chicago, Chicago, Illinois 60607, USA. [39]Southern Connecticut State University, New Haven, Connecticut 06515, USA. [40]Purdue University, West Lafayette, Indiana 47907, USA. [41]Valparaiso University, Valparaiso, Indiana 46383, USA. [42]Warsaw University of Technology, Warsaw 00-661, Poland. [43]Temple University, Philadelphia, Pennsylvania 19122, USA. [44]National Cheng Kung University, Tainan 70101, Taiwan. [45]Indiana University, Bloomington, Indiana 47408, USA. [46]Frankfurt Institute for Advanced Studies (FIAS), Frankfurt 60438, Germany. [47]Argonne National Laboratory, Argonne, Illinois 60439, USA. [48]Institute of Physics, Bhubaneswar 751005, India. [49]Pusan National University, Pusan 46241, Korea. [50]Institute of Nuclear Physics, PAN, Cracow 31-342, Poland. [51]Max-Planck-Institut fur Physik, Munich 80805, Germany. [52]Michigan State University, East Lansing, Michigan 48824, USA. [53]World Laboratory for Cosmology and Particle Physics (WLCAPP), Cairo 11571, Egypt. [54]United States Naval Academy, Annapolis, Maryland 21402, USA.

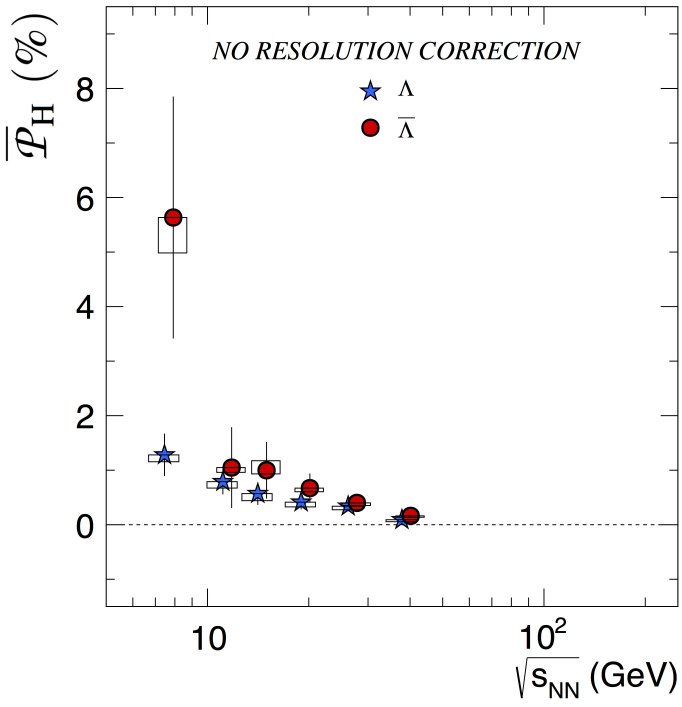

Extended Data Figure 1 | The uncorrected average polarization in Au + Au collisions. The polarization signal plotted in Fig. 4 is plotted without applying the reaction-plane resolution correction. As in Fig. 4, statistical uncertainties are indicated by error bars, while boxes indicate systematic uncertainty. Although the number of particles used to estimate $\phi_{j_{sys}}$ increases with the energy of a collision, the resolution ($R_{EP}^{(1)}$) with which $\phi_{j_{sys}}$ is estimated actually decreases with increasing $\sqrt{s_{NN}}$. This is because the strength of the momentum–space anisotropy (called 'directed flow') generated in the collision is greater[22] at low $\sqrt{s_{NN}}$. Therefore, the polarization signal falls more steeply with $\sqrt{s_{NN}}$ if the resolution correction is not applied. The uncorrected signal is shown in Extended Data Fig. 1, which may be compared to Fig. 4. Since for a given $\sqrt{s_{NN}}$, $R_{EP}^{(1)}$ varies slightly with collision multiplicity, the raw signal is measured separately for three bins in centrality (20–30%, 30–40% and 40–50%). These are each corrected with the corresponding resolution factor, and a weighted sum is reported in Fig. 4.